npj | quantum information

Article

Published in partnership with The University of New South Wales

https://doi.org/10.1038/s41534-024-00867-0

Scalable determination of multipartite entanglement in quantum networks

Wei-Ting Kao[1,2,8], Chien-Ying Huang[3,4,8], Tung-Ju Tsai[1,2], Shih-Hsuan Chen[1,2], Sheng-Yan Sun[1,2], Yu-Cheng Li[1,2], Teh-Lu Liao[1], Chih-Sung Chuu[5,6], He Lu[7] & Che-Ming Li[1,2] ✉

Quantum networks comprised of entangled end nodes serve stronger than the classical correlation for unparalleled quantum internet applications. However, practical quantum networking is affected by noise, which at its worst, causes end nodes to be described by pre-existing classical data. In such untrusted networks, determining quantum network fidelity and genuine multi-node entanglement becomes crucial. Here, we show that determining quantum network fidelity and genuine N-node entanglement in an untrusted star network requires only $N + 1$ measurement settings. This method establishes a semi-trusted framework, allowing some nodes to relax their assumptions. Our network determination method is enabled by detecting genuine N-node Einstein-Podolsky-Rosen steerability. Experimentally, using spontaneous parametric down-conversion entanglement sources, we demonstrate the determinations of genuine 3-photon and 4-photon quantum networks and the false positives of the widely used entanglement witness, the fidelity criterion of 1/2. Our results provide a scalable method for the determination of multipartite entanglement in realistic quantum networks.

Quantum networks[1–3] aim to provide networking nodes with the ability to process quantum information jointly, extending beyond point-to-point communication. This capability relies on quantum entanglement between the end nodes. With entanglement, quantum networks benefit from quantum correlation, coordination, and security[3–17]. Therefore, quantum networks are expected to enable applications that fundamentally enhance classical networks and serve as the building blocks of a quantum internet[18–37].

Inevitable errors or imperfections, however, exist in required hardware components. Moreover, qubits are fragile when subjected to environmental noise. These factors can result in discrepancies between the actual networks and their target configurations. In particular, the damages can make the end nodes classical as pre-existing classical data at worst. Typically, networking participants have limited knowledge regarding such node information, rendering both the network nodes and the networking implementations untrusted from the perspective of end-users[38–40].

Evaluating the created networks under untrusted conditions of end nodes and hardware components is essential for realistic quantum networking. This assessment is necessary to determine whether the entanglement backbone, which underlies each quantum network stage in developing an ultimate quantum internet[1–3], has been faithfully established. Quantum network fidelity, also referred to as quantum fidelity or simply fidelity, is essential for evaluating the closeness of a created network state to a target state. For example, fidelity can be used to construct an entanglement witness (EW)[41–45] to detect genuine multi-node entanglement. However, employing EWs to determine network fidelity and genuine multi-node entanglement requires assuming trusted measurement devices that adhere to the principles of quantum mechanics, rather than blindly outputting pre-existing classical data. Therefore, EWs are not applicable for determining the untrusted networking scenario.

The challenge of distrust can be tackled through self-testing analysis[46–48]. However, this method only provides an estimate of the lower bound of the fidelity to the target state up to local isometries. Interestingly, Lu et al.[40] demonstrated that the network fidelity could be measured in the presence of untrusted end nodes if the fidelity value exceeds the threshold for genuine multi-node Einstein-Podolsky-Rosen (EPR) steering. This approach to network determination is distinct from all other known steering identification methods[38,49–51].

Furthermore, as quantum networking scales up in size, the functionality of the quantum network unveils the true power of quantum application protocols, making them increasingly superior to classical networks[1–3]. However, the challenge persists on how to conduct the necessary network determination in the presence of untrusted measurement devices with

[1]Department of Engineering Science, National Cheng Kung University, Tainan, 70101, Taiwan. [2]Center for Quantum Frontiers of Research and Technology, National Cheng Kung University, Tainan, 70101, Taiwan. [3]Department of Electrical Engineering, California Institute of Technology, Pasadena, CA, 91125, USA. [4]Institute for Quantum Information and Matter, California Institute of Technology, Pasadena, CA, 91125, USA. [5]Department of Physics, National Tsing Hua University, Hsinchu, 30013, Taiwan. [6]Center for Quantum Science and Technology, Hsinchu, 30013, Taiwan. [7]School of Physics, Shandong University, Jinan, 250100, China. [8]These authors contributed equally: Wei-Ting Kao, Chien-Ying Huang ✉e-mail: cmli@mail.ncku.edu.tw

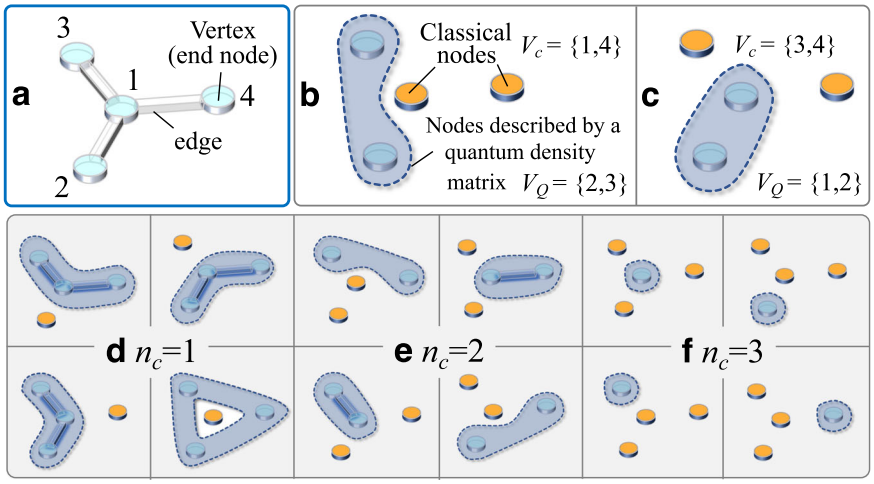

Fig. 1 | Distinction between quantum networks and untrusted quantum-classical hybrids. Vertices and edges in a star topology represent an N-node entangled network equivalent to a GHZ state[59], as illustrated in **a** for $N = 4$. The former stand for end nodes (qubits), and the latter describe node-node quantum interaction. **b** A classical-quantum hybrid consists of classical nodes of pre-existing data R_{m_k} which constitute a fixed measurement set $\mathbf{v}_k$ and nodes described by a density matrix of quantum mechanics. See Eq. (4). A variant can be found according to the number of classical (quantum) nodes, n_c ($N - n_c$), and the combination of classical (quantum) end nodes described by the node index set V_c (V_Q), such as (c). For $0 < n_c < 4$, all possible hybrids are shown in **b**–**f**. We show detection of N-node star-topology quantum networks by ruling out all quantum-classical hybrids requires only $N + 1$ measurement settings.

minimal experimental efforts. From a scalability standpoint, the practical steps in local measurement settings (the settings of simultaneous measurement of single qubit operators in parallel[41]) in the current network determination based on steering[40] still exhibit exponential growth with the number of end nodes.

In this work, we address the issue of distrust and scalability in network determination by detecting genuine N-node EPR steering in a scalable manner. This method establishes a semi-trusted framework, allowing some nodes to relax their assumptions. With only $N+1$ measurement settings, our fidelity criterion enables determining network fidelity and genuine multi-node entanglement in star network topology or Greenberger-Horne-Zeilinger (GHZ) state under untrusted conditions (Fig. 1). This makes our scalable network determination method useful for entanglement distribution in realistic quantum networks. The GHZ state, although not utilized in certain quantum networks such as those constructed by entangled qubit pairs[52–56], has played a significant and central role in various crucial quantum networking tasks. For example, the GHZ state is the resource for achieving quantum secret sharing[4–8,39] and performing one-way quantum computing[57]. Moreover, the GHZ state is the backbone for quantum distributed sensing[9,10] and quantum conference key agreement and distribution[15–17]. It even serves as the building block of genuine quantum networks with superposed tasks and addressing[58]. Therefore, our formalism and the corresponding experimental demonstration help realize these assignments in quantum networks in the presence of uncharacterized network nodes.

Results

Scalable network determination method

Suppose an N-node network is prepared according to an N-qubit graph state in a star topology[59]: $|S_N\rangle = (|0\rangle_1 \otimes_{k=2}^N |+\rangle_k + |1\rangle_1 \otimes_{k=2}^N |-\rangle_k)/\sqrt{2}$, under the first node as the center [Fig. 1a], or equivalently a GHZ state: $|G_N\rangle = (\otimes_{k=1}^N |0\rangle_k + \otimes_{k=1}^N |1\rangle_k)/\sqrt{2}$, where $|\pm\rangle_k = (|0\rangle_k \pm |1\rangle_k)/\sqrt{2}$ and $\{|0\rangle_k \equiv |0\rangle, |1\rangle_k \equiv |1\rangle\}$ is an orthonormal basis. The fidelity of a created network described by a density operator ρ_{expt} and the target state $|\psi\rangle$ is defined by: $F = \text{tr}(\rho_{\text{expt}}|\psi\rangle\langle\psi|)$, for $|\psi\rangle = |S_N\rangle, |G_N\rangle$. To measure fidelity by the remote end-users, we decompose the projector into a linear combination of tensor products of N local observables: $|\psi\rangle\langle\psi| = \sum_{\vec{m}} h_{\vec{m}} \otimes_{k=1}^N \hat{R}_{m_k}$, where $\hat{R}_{m_k}$ represents the m_kth observable of the kth qubit (end node) and $\vec{m} \equiv (m_1, \ldots, m_N)$ describes the type of N-observable setting. The decomposition of the star-graph state or the GHZ state is not unique and decides the coefficients $h_{\vec{m}}$. To emphasize how F can be measured, we rephrase the fidelity as the following fidelity function:

$$F(N) = \sum_{\vec{m}} h_{\vec{m}} \left\langle R_{m_1} \ldots R_{m_N} \right\rangle, \tag{1}$$

where R_{m_k} is the outcome of the m_kth measurement on the kth end node and $\left\langle R_{m_1} \ldots R_{m_N} \right\rangle$ denote the mean value of the product of N measurement outcomes. The number of local measurement settings required to measure the fidelity $F(N)$ depends on the local measurements required to determine the expectation values, $\left\langle R_{m_1} \ldots R_{m_N} \right\rangle$.

When using the fidelity EW for entanglement detection, the ρ_{expt} is detected as being genuinely N-qubit entangled if the measured fidelity satisfies the criterion $F(N) > \max_{\rho_B} \sum_{\vec{m}} h_{\vec{m}} \text{tr}(\rho_B \otimes_{k=1}^N \hat{R}_{m_k}) = 1/2$[43,60], which excludes the possibility of a biseparable state ρ_B. The number of local measurement settings required to obtain all the $\left\langle R_{m_1} \ldots R_{m_N} \right\rangle$ affects the experimental efforts of determining F and entanglement. When the measurements on each qubit are performed with the observables of the Pauli matrices, the total number of measurement settings is $2^{N-1} + 1$[40]. Whereas Gühne et al.[61] show that this experimental effort can be small to $N+1$ local measurement settings by introducing measurements in the x-y-plane of the Bloch sphere. This seminal determination method has been widely used in a range of multipartite entanglement experiments; see, for example, the recent determination in refs. 48,62,63.

Pre-existing classical data from classical end nodes or untrusted measurement devices can cause the resulting fidelity to be unreliable and lead to false positives of EW-based entanglement detection in quantum networks, as we will demonstrate below. We eliminate the classical possibilities and maintain the scalability of entanglement detection[61] by characterizing genuine N-node EPR steering via the following end-node observables.

(i) $|S_N\rangle$:

$$\begin{aligned}
\hat{R}_{m_1} &= \cos\left(\tfrac{m_1\pi}{N}\right) X + \sin\left(\tfrac{m_1\pi}{N}\right) Y,\ m_1 = 1, 2, \ldots, N, \\
\hat{R}_{m_1} &= Z,\ m_1 = N+1, \text{ and} \\
\hat{R}_{m_k} &= \cos\left(\tfrac{m_k\pi}{N}\right) Z - \sin\left(\tfrac{m_k\pi}{N}\right) Y,\ m_k = 1, 2, \ldots, N, \\
\hat{R}_{m_k} &= X,\ m_k = N+1, \qquad \text{for } k = 2, 3, \ldots, N,
\end{aligned} \tag{2}$$

where X, Y and Z are the Pauli-x, Pauli-y, and Pauli-z matrices respectively, and X and Y are defined via their relations to $Z \equiv |0\rangle\langle 0| - |1\rangle\langle 1|$.

(ii) $|G_N\rangle$:

$$\begin{aligned}
\hat{R}_{m_k} &= \cos\left(\tfrac{m_k\pi}{N}\right) X + \sin\left(\tfrac{m_k\pi}{N}\right) Y,\ m_k = 1, 2, \ldots, N, \\
\hat{R}_{m_k} &= Z,\ m_k = N+1, \qquad \text{for } k = 1, 2, \ldots, N.
\end{aligned} \tag{3}$$

Equations (2) and (3) and the identity operator $\hat{R}_0 = I$ constitute the target state $|\psi\rangle$, requiring only $N + 1$ observables for each end node.

Experimentally, using $N+1$ measurement settings is sufficient to perform the fidelity measurements (1)[61]. See Supplementary Note 1 for concrete examples of decomposing the target GHZ states with $N+1$ observables for fidelity measurements by $N+1$ local measurement settings. Note that Eqs. (2) and (3) are equivalent up to $N-1$ Hadamard transformations. This can be seen from their structures of state vectors $|S_N\rangle$ and $|G_N\rangle$.

The ρ_{expt} possesses genuine N-node EPR steerability close to $|\psi\rangle$ if the measured fidelity is larger than the maximum fidelity a network's measurement results mixed with the pre-existing classical data can achieve, namely

$$F(N) > \mathcal{F}_c \equiv \max_{V_c} \sum_{\vec{m}} h_{\vec{m}} \left\langle \bigotimes_{k\in V_Q} \hat{R}_{m_k} \right\rangle \prod_{k\in V_c} R_{m_k}, \tag{4}$$

where V_c denotes the index set of classical end nodes, and V_Q is the index set of the rest nodes described in quantum density matrix. See Fig. 1b–f for classical-quantum hybrids consisting of classical nodes of pre-existing data R_{m_k} and nodes described by a density matrix of quantum mechanics. As shown in Eq. (1), $h_{\vec{m}}$ represents the decomposition coefficients of target state $|S_N\rangle$ or $|G_N\rangle$ with observables (2) or (3), respectively. $\hat{R}_{m_k}$ is the m_kth local observable of the kth end node belonging to V_Q and following quantum mechanics. A classical end node, say the kth node, has physical properties independent of observation and can be specified by a fixed set of measurement outcomes, $\mathbf{v}_k \equiv \{R_{m_k} | m_k = 1, 2, \ldots, N+1\}$ where $R_{m_k} \in \{+1, -1\}$ corresponding to the observables (2) or (3)[64]. Here, the pre-existing classical data R_{m_k} is a characteristic of a classical system. The value of the pre-existing classical data $+1$ or -1 represents the state of a physical property and exists before the property's measurement, independent of the observation. When considering several physical properties corresponding to observables in quantum mechanics, their classical pre-existing data constitute the pre-existing and fixed set $\mathbf{v}_k$ that can describe the classical system. Such a classical state can be considered a pre-existing recipe fully specifying how the classical system behaves. The feature of pre-existing measurement outcomes and independent observations is also called the assumption of realism[64–66]. Therefore, we use the realism assumption, i.e., the pre-existing data, to define and describe a node classical in noisy networks. Supplementary Note 2 provides the details of pre-existing classical data in classical nodes. The fixed set $\mathbf{v}_k$ consisting of the pre-existing classical data R_{m_k} under the assumption of realism has been used to calculate the fidelity upper bound, $\mathcal{F}_c$, for classical-quantum hybrids in Eq. (4). As will be introduced below, we will see how the $\mathbf{v}_k$ is used to discuss and determine $\mathcal{F}_c$.

Explicitly, the maximization for $\mathcal{F}_c$ in Eq. (4) is over all the parameters related to V_c, including the classical end node number, n_c, for $0 < n_c < N$, the combinations of these classical nodes, their pre-existing classical data of $\mathbf{v}_k$, and the states of the quantum end nodes in V_Q. Therefore, we have

$$\mathcal{F}_c = \max_{n_c, \{\mathbf{v}_k | k\in V_c\}} E\left[\sum_{\vec{m}} h_{\vec{m}} \bigotimes_{k\in V_Q} \hat{R}_{m_k} \prod_{k\in V_c} R_{m_k}\right], \tag{5}$$

where $E[\cdot]$ denotes the largest eigenvalue of the operator. After a careful derivation and calculation, we arrive at the following results:

$$\begin{aligned} \mathcal{F}_c(N) &= \frac{1+\sqrt{1+4\frac{\csc^2\left(\frac{\pi}{2N}\right)}{N^2}}}{4} \quad \text{odd } N, \\ \mathcal{F}_c(N) &= \frac{1+\sqrt{3}}{4} \simeq 0.683 \quad \text{even } N. \end{aligned} \tag{6}$$

$\mathcal{F}_c$ with odd N is monotonically decreasing: $\mathcal{F}_c(3) \simeq 0.667$, $\mathcal{F}_c(5) \simeq 0.6589$, and $\lim_{N\to\infty} \mathcal{F}_c(N) \simeq 0.6547$. Note that the equivalence between Eq. (2) and Eq. (3) leads to the same upper bounds $\mathcal{F}_c$ for the target states $|S_N\rangle$ and $|G_N\rangle$. To obtain Eq. (6) from Eq. (5), we first evaluate the maximum fidelity of $|G_N\rangle$ and an N-node network with n_c classical nodes: $\mathcal{F}_{n_c}(N) = \max_{\{\mathbf{v}_k | k\in V_c, |V_c|=n_c\}} F(N)$. Then we consider all cases where the classical nodes exist in the created network and define the maximum value of the calculated fidelities $\mathcal{F}_{n_c}(N)$ as $\mathcal{F}_c(N)$. See Supplementary Note 3 for the detailed derivation procedure of these two steps. In Supplementary Note 4, the noise tolerance of the steering criterion (4) is discussed as well.

The criterion for genuine multi-node EPR steering (4) is stricter than the criterion for genuine multipartite entanglement. That is, the classical upper bounds (6) imply $\mathcal{F}_c(N) > 0.5$, which results in false positives using EW-based entanglement detection in untrusted networks[44,45]. A false positive entanglement detection means a result of an EW-based entanglement test that appears to show genuine multipartite entanglement exists or is present when this is not correct. Determining network fidelity and genuine multi-node entanglement using EWs requires the assumption of trusted measurement devices that follow quantum mechanics, not outputting pre-existing classical data. Therefore, a false positive entanglement detection may occur when untrusted nodes exist in networks. As found and presented in our work, networks in the presence of classical nodes enable passing the EW-based entanglement test, which causes the false positive of genuine multipartite entanglement. As the criterion (4) detects the steerability of ρ_{expt}, the possibilities of the pre-existing classical measurement outcomes from classical end nodes or untrusted measurement devices are ruled out. Therefore, the quantum network fidelity is reliably determined under untrusted measurements, and genuine multi-node entanglement is also detected.

Furthermore, our network determination method only requires $N+1$ measurement settings, which is notably different from the existing method that requires $2^{N-1}+1$ measurement settings[40]. For both works, the underlying concept and method to derive the maximum fidelity of networks with classical nodes depend on two items: (1) the observables used for the state decomposition of the target state, and (2) the calculation of the maximum fidelity for classical-quantum hybrids consisting of classical nodes of pre-existing data R_{m_k} which constitute a fixed measurement set $\mathbf{v}_k$ and nodes described by a density matrix of quantum mechanics. Lu et al.[40] used Pauli matrices as observables, forming an orthonormal set resembling typical quantum state tomography. When employing orthogonal observables, the maximum fidelity of quantum-classical hybrid networks decreases monotonically with increasing classical nodes, providing a scale for network imperfections. Our method uses observables lacking this orthogonality. Explicitly, the maximum fidelity remains and does not change with the classical node number under a given odd total node number. Maximum fidelity changes with the classical node number for a given even total node number, but the fidelity value does not decrease monotonically. Moreover, the fidelity value maximized over all classical node numbers does not change with the even total node number, whereas this maximum fidelity monotonically decreases with the odd total node number. See Supplementary Table 1 for concrete examples. Without orthonormal observables, maximum fidelities do not strictly decrease with classical node count. However, the trade-off for having a scale to indicate the degree of network imperfection is the exponential increase in required measurement settings with the number of network nodes. In contrast, our method only requires a linearly increasing number of measurement settings. For a more detailed comparison between both works, see Supplementary Note 5.

Experimental demonstration of genuine *N*-node EPR steering

Experimentally, without loss of generality, we demonstrate the determination of genuine 3-node and 4-node quantum networks with EPR steering in GHZ states for the equivalence between $|S_N\rangle$ and $|G_N\rangle$. We created two spontaneous parametric down-conversion (SPDC) sources of polarization-entangled photon pairs and an interferometer[67,68] to generate a multi-photon entanglement source. See Methods for more experimental details. A schematic diagram of the experimental setup is shown in Fig. 2. We first implemented the determination of the steerability in the created 3-photon and 4-photon states, ρ_{expt,G_3} and ρ_{expt,G_4}, respectively. With state decomposition according to (3), we performed required measurements on our

created states

$$F(3)=\frac{1}{8}\left(1+\sum_{\pi}\langle R_0R_4R_4\rangle\right)+\frac{1}{6}\sum_{k=1}^{3}(-1)^k\langle R_kR_kR_k\rangle, \tag{7}$$

$$F(4)=\frac{1}{16}\left(1+\langle R_5R_5R_5R_5\rangle+\sum_{\pi}\langle R_0R_0R_5R_5\rangle\right)+\frac{1}{8}\sum_{k=1}^{4}(-1)^k\langle R_kR_kR_kR_k\rangle, \tag{8}$$

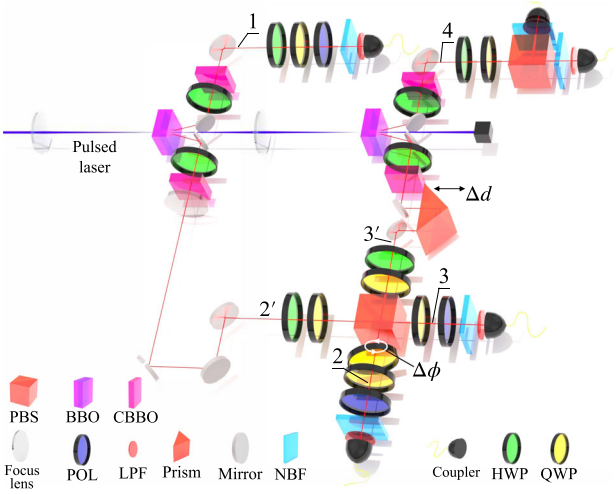

Fig. 2 | Experimental setup for scalable determination of multi-photon entanglement in quantum networks. A SPDC photon source consists of a BBO crystal and a compensator [a CBBO and a half wave plate (HWP)] pumped with a pulsed laser beam. To generate multi-photon entanglement, two SPDC photon sources were created, and photons in modes 2′ and 3′ interfere with a PBS under good spatial and temporal overlap. Photons were selected by the narrow-band filter (NBF) and long-pass filter (LPF), collected by fiber couplers and detected by silicon avalanche single-photon detectors (not shown).

where $\sum_{\pi}$ denotes the sum over all the permutations of the nodes. Measuring $F(3)$ and $F(4)$ requires only 4 and 5 measurement settings, respectively. (See Supplementary Note 1.) The experimental results are summarized in Fig. 3a, b. We generated ρ_{expt,G_3} and ρ_{expt,G_4} with $F_{G_3}(3)=(78.00\pm0.60)\%>\mathcal{F}_c(3)\simeq0.667$, and $F_{G_4}(4)=(75.79\pm0.37)\%>\mathcal{F}_c(4)\simeq0.683$, respectively. Our demonstrations with only $N+1$ measurement settings thus determine genuine three-photon and four-photon steerability according to the criteria (4). To demonstrate that the previous method[40] requires more local measurement settings, we also obtained similar fidelities to satisfy the trustiness tests with $2^{N-1}+1$ Pauli observables. We obtained $F_{G_3}(3)=(77.93\pm0.62)$ and $F_{G_4}(4)=(75.84\pm0.31)$ using 5 and 9 local measurement settings, respectively. See Supplementary Note 8 for details of Pauli observables measurement. This shows the improved scalability of our network determination method.

False positives of EW-based entanglement detection

Ruling out the classical-quantum hybrid networks (Fig. 1) with the fidelity criterion (4) represents genuine N-node entanglement in quantum networks where any classical means is impossible. One concrete illustration is to rule out the best fidelity mimicry using the pre-existing classical data that can enable false positives using EW-based entanglement detection. To experimentally demonstrate the false positives of EW-based entanglement detection in $N=3$ and $n_c=1$ network, we created a 2-photon state mixed with pre-existing classical data from 1 classical node. This quantum-classical hybrid was created according to the one which can achieve the best fidelity mimicry $\mathcal{F}_c(3)\simeq0.667$ [Eq. (6)]. See Methods for more details about the preparation and measurement of quantum-classical hybrids. As shown in Fig. 4a, we observed the fidelity of the quantum-classical hybrid $F_{c_1}(3)=(61.05\pm0.44)\%$, which is greatly larger than the widely used EW fidelity criterion of 1/2 for the detection of genuine N-node entanglement[42–45]. Whereas the created 2-photon state mixed with 1 classical node shows the false positive of detecting genuine 3-node entanglement using EW-based entanglement detection. Our fidelity criterion through $\mathcal{F}_c(3)$ rules out the mimicry of genuine 3-node entanglement with a quantum-classical hybrid.

Similarly, we created $N=4$ quantum-classical hybrid networks using 2-photon state and 1-photon state for $n_c=2$ and $n_c=3$, respectively. We

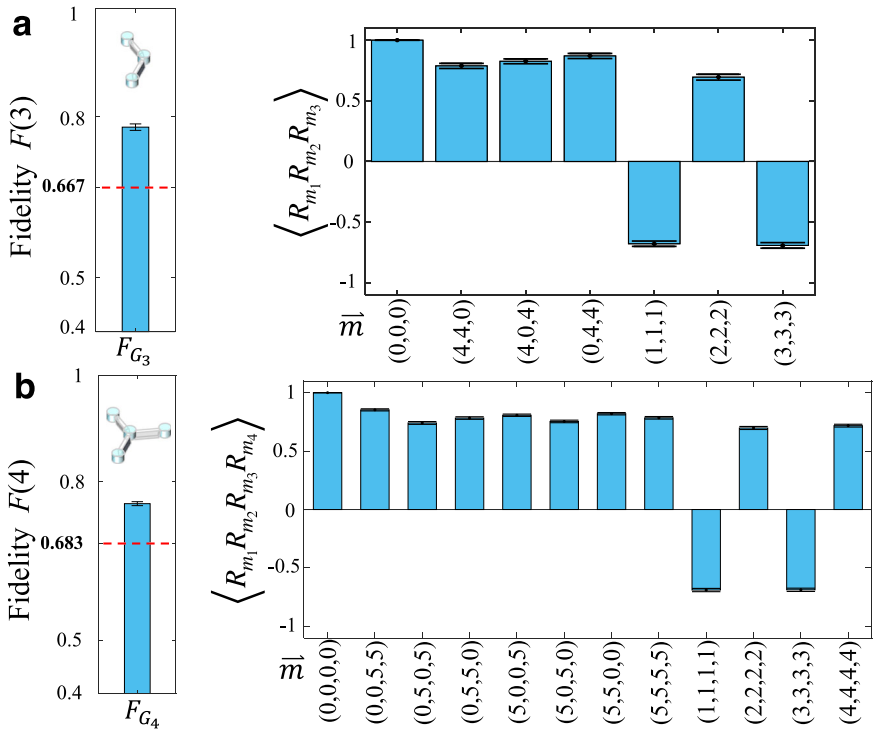

Fig. 3 | Experimental genuine N-photon EPR steerability. We observed the experimental fidelities of (**a**) $F_{G_3}(3)=(78.00\pm0.60)\%$, and (**b**) $F_{G_4}(4)=(75.79\pm0.37)\%$, where the error bars represent the standard deviation of the measured photon counts based on Poissonian statistics. They reveal that the created photons possess genuine N-node EPR steerability under scalable $N+1$ measurement settings. Then the entanglement creation and fidelity measurements can be trusted without calibration or knowledge of all the running experimental apparatus.

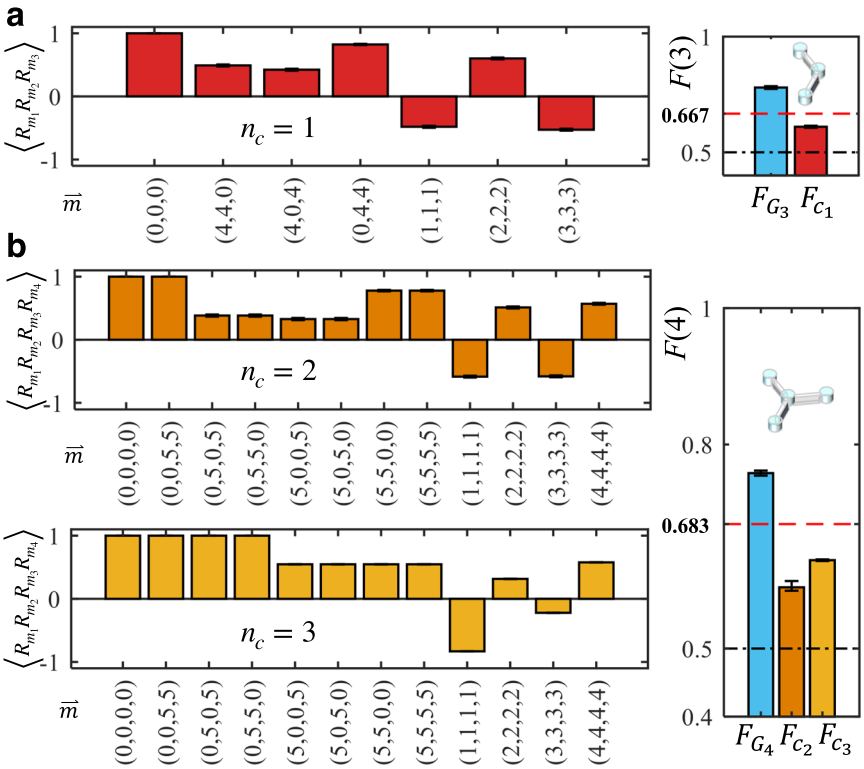

Fig. 4 | False positives of EW-based entanglement detection. a For $N = 3$, the experimental network mixed with one classical node ($n_c = 1$) has the fidelity, $F_{c_1}(3) = (61.05 \pm 0.44)\%$, larger than than the upper bound of 1/2 ruled out by EW-based entanglement detection. This quantum-classical hybrid was created according to the one which can achieve $\mathcal{F}_c(3) \simeq 0.667$ [Eq. (6)]. **b** For $N = 4$, the fidelities of the two demonstrated quantum-classical hybrid networks: $F_{c_2}(4) = (59.21 \pm 0.72)\%$ and $F_{c_3}(4) = (62.99 \pm 0.12)\%$, for $n_c = 2$ and $n_c = 3$, respectively, are larger than 1/2 and smaller than $\mathcal{F}_c(4) \simeq 0.683$ [Eq. (6)], where the network with three classical nodes has better ability of mimicking $|G_4\rangle$. These two hybrids were created aiming for the best simulations with two and three classical nodes, respectively. The error bars represent the measured photon counts' standard deviation based on Poissonian statistics.

observed the fidelities $F_{c_2}(4) = (59.21 \pm 0.72)\%$ and $F_{c_3}(4) = (62.99 \pm 0.12)\%$, for $n_c = 2$ and $n_c = 3$, respectively, which are larger than 1/2 and smaller than $\mathcal{F}_c(4) \simeq 0.683$, as shown in Fig. 4b, c. Our demonstrations validated the false positives of EW-based entanglement detection and the practicality of our determination method in quantum networks. It is worth emphasizing that environmental noise or experimental imperfections are generally unknown in realistic networking, and more than one such extreme case, including their mixtures, must be excluded. Therefore satisfying the fidelity criterion (4) becomes significant to rule out all possibilities of false positives.

Discussion

The presented results provide an efficient method for the determination the quantum network fidelity and genuine multi-node entanglement in the presence of untrusted nodes with the minimum experimental effort in existing protocols. They benefit from detecting genuine N-node EPR steering in star topology networks with only $N + 1$ measurement settings in a semi-trusted framework where some nodes can relax their quantum mechanical assumptions. The proof-of-principle photonic network experiments validate that the maximum fidelity obtained from the combination of measurement results of trusted nodes and the pre-existing classical data can surpass the widely used fidelity criterion of 1/2[42–45]. This clearly shows the false positives of EW-based entanglement detection in the presence of untrusted measurement devices. Our results, therefore, offer a scalable manner to faithfully determine multipartite entanglement in quantum networks and insights into evaluating the entanglement backbone in realistic quantum networks[18–37]. We expect our method could be extended to other types of network topology for generic quantum internet with further studies.

Methods

Multi-photon entanglement source

The two SPDC sources were pumped with a pulsed laser beam (center wavelength 390 nm, pulse duration 144 fs, repetition rate 76 MHz, and average power 1.0 W). In each source, a β-barium-borate (BBO) crystal (2 mm) was pumped to generate pairs of polarization-entangled photons by type-II non-collinear SPDC, including the compensation for the walk-off effect by an additional BBO crystal (CBBO, 1 mm). See Fig. 2 for the experimental setup. Supplementary Note 6 details the laser system and photon source. The prepared two photon pairs in modes 1-2′ and 3′-4 have an average creation rate of ~99×10^3 pairs per second and an average fidelity of $(93.61 \pm 0.09)\%$ close to $|\Phi^+\rangle = (|HH\rangle + |VV\rangle)/\sqrt{2}$, where $|H\rangle \equiv |0\rangle$ ($|V\rangle \equiv |1\rangle$) denotes the horizontal (vertical) photon polarization state. Then, photons in modes 2′ and 3′ were made to temporally and spatially overlap[69] at a polarizing beam splitter (PBS) by fine-tuning the delay Δd. The observed visibility of the Hong-Ou-Mandel (HOM) type interference fringes is better than 76%. Supplementary Note 7 provides more details of HOM experiments. By properly tuning the angle $\Delta\phi$ of the quarter wave plate (QWP) around its vertically-oriented fast axis and after post-selected four-fold coincidence detection, a four-photon experimental state ρ_{expt,G_4} in mode 1-2-3-4 was created at a rate of ~76 events per second. A three-photon state ρ_{expt,G_3} in mode 2-3-4 was generated in the same manner as the photon in mode 1 was measured as a trigger.

Preparation and measurement of quantum-classical hybrids

To experimentally create quantum-classical hybrids for false positives of EW-based entanglement detection, we prepared the eigenstates under specific conditions of V_c and $\{\mathbf{v}_k | k \in V_c\}$ for the fidelity operator $\hat{F}_{n_c}(N)$ (see Eq. (16) in Supplementary Note 3), which correspond to the best fidelity mimicry of the target state $|G_N\rangle$. For $N = 3$ and $n_c = 1$ network with the state decomposition of $|G_3\rangle$ (see Eq. (4) in Supplementary Note 1), we have the fidelity operator $\hat{F}_{n_c}(N)$ for a two-photon state in modes 3 and 4, under the classical node in mode 2 of $\mathbf{v}_2 = \{+1, +1, +1, +1\}$ (see Eq. (9) in Supplementary Note 2),

$$\hat{F}_1(3) = \frac{1}{8}(I \otimes I + I \otimes Z + Z \otimes Z + Z \otimes I) + \frac{1}{6}(-\hat{R}_1 \otimes \hat{R}_1 + \hat{R}_2 \otimes \hat{R}_2 - \hat{R}_3 \otimes \hat{R}_3). \quad (9)$$

We then created two-photon state in modes 3 and 4 according to the eigenvector with the maximum eigenvalue $\mathcal{F}_1(3)$ of Eq. (9). Explicitly, such an eigenvector is of the form:

$$|e_1(3)\rangle = \frac{1}{\sqrt{|\alpha|^2+1}}(\alpha|HH\rangle + |VV\rangle), \tag{10}$$

where $\alpha = -1 + i\sqrt{3}$. Note that under this condition, $\mathcal{F}_1(3) = \mathcal{F}_c(3) \simeq 0.667$. Supplementary Note 3 provides the detailed derivation of $\mathcal{F}_c$ [Eq. (6)] from $\hat{F}_{n_c}(N)$. Experimentally, the two-photon state was created by measuring the photon in mode 2 of the state $\rho_{\text{expt},G3}$ via a QWP setting at −16.85° and a polarizer (POL) setting at 5.08° (Fig. 2). With $\mathbf{v}_2 = \{+1, +1, +1, +1\}$ we observed a fidelity of $F_{c_1} = (61.05 \pm 0.44)\%$, which is larger than the upper bound of 1/2 ruled out by EW-based entanglement detection .

As the same method used above, for $N = 4$ and $n_c = 2$, with the state decomposition of $|G_4\rangle$ and $\mathbf{v}_1 = \{+1, +1, +1, +1, +1\}$ and $\mathbf{v}_2 = \{-1, +1, +1, -1, +1\}$ (see Eqs. (5) and (10) in Supplementary Note 2) we can write the fidelity operator $\hat{F}_{n_c}(N)$ for a two-photon state in modes 3 and 4,

$$\begin{aligned}\hat{F}_2(4) = &\frac{1}{16}(I\otimes I + I\otimes I + I\otimes Z + I\otimes Z + Z\otimes I + Z\otimes Z + Z\otimes I + Z\otimes Z)\\ &+\frac{1}{8}(\hat{R}_1\otimes\hat{R}_1 + \hat{R}_2\otimes\hat{R}_2 - \hat{R}_3\otimes\hat{R}_3 - \hat{R}_4\otimes\hat{R}_4).\end{aligned} \tag{11}$$

We then generated a two-photon state in modes 3 and 4 according to the eigenvector of $\hat{F}_2(4)$ with the maximum eigenvalue, $\mathcal{F}_2(4) = \mathcal{F}_c(4) \simeq 0.683$:

$$|e_2(4)\rangle = \frac{1}{\sqrt{|\beta|^2+1}}(\beta|HH\rangle + |VV\rangle), \tag{12}$$

where $\beta = (1+\sqrt{3})e^{i\pi/4}/\sqrt{2}$. The two-photon state was created by measuring the photon in mode 2 of the state $\rho_{\text{expt},G3}$ by setting QWP and POL at 25.18° and 34.02°, respectively. Combined with $\mathbf{v}_1 = \{+1, +1, +1, +1, +1\}$ and $\mathbf{v}_2 = \{-1, +1, +1, -1, +1\}$, the experimental value of the fidelity is $F_{c_2} = (59.21 \pm 0.72)\%$, which shows the false positive of detecting genuine 3-node entanglement using EW-based entanglement detection.

Furthermore, we demonstrated the false positives of EW-based entanglement detection by creating a state close to a target of one photon in mode 1:

$$|e_3(4)\rangle = \frac{1}{\sqrt{|\gamma|^2+1}}(\gamma|H\rangle + |V\rangle), \tag{13}$$

where $\gamma = [2+\sqrt{2(4+\sqrt{2})}]/(1+\sqrt{2}+i)$, and three classical nodes with the states $\mathbf{v}_2 = \{+1, +1, +1, +1, +1\}$, $\mathbf{v}_3 = \{+1, +1, +1, +1, +1\}$ and $\mathbf{v}_4 = \{-1, +1, +1, +1, -1\}$ (see Eq. (10) in Supplementary Note 2), which provides $\mathcal{F}_3(4) \simeq 0.661$. Such a state was prepared by setting QWP and POL at 0° and 27.38°, respectively, and then measuring the photon in mode 2′ of the experimental two-photon state, $\rho_{\text{expt},\Phi^+}$. With the created state, we observed $F_{c_3} = (62.99 \pm 0.12)\%$, which demonstrated the false positive of EW-based entanglement detection.

Data availability

The data supporting the findings of this study are available from the corresponding author upon reasonable request.

Code availability

The code supporting the findings of this study is available from the corresponding author upon reasonable request.

Received: 28 September 2023; Accepted: 29 July 2024;
Published online: 08 August 2024

References

1. Kimble, H. J. The quantum internet. *Nature* **453**, 1023–1030 (2008).
2. Ritter, S. et al. An elementary quantum network of single atoms in optical cavities. *Nature* **484**, 195–200 (2012).
3. Wehner, S., Elkouss, D. & Hanson, R. Quantum internet: A vision for the road ahead. *Science* **362**, eaam9288 (2018).
4. Hillery, M., Bužek, V. & Berthiaume, A. Quantum secret sharing. *Phys. Rev. A* **59**, 1829–1834 (1999).
5. Chen, Y.-A. et al. Experimental quantum secret sharing and third-man quantum cryptography. *Phys. Rev. Lett.* **95**, 200502 (2005).
6. Markham, D. & Sanders, B. C. Graph states for quantum secret sharing. *Phys. Rev. A* **78**, 042309 (2008).
7. Bell, B. A. et al. Experimental demonstration of graph-state quantum secret sharing. *Nat. Commun.* **5**, 5480 (2014).
8. Lu, H. et al. Secret sharing of a quantum state. *Phys. Rev. Lett.* **117**, 030501 (2016).
9. Kómár, P. et al. A quantum network of clocks. *Nat. Phys.* **10**, 582–587 (2014).
10. Proctor, T. J., Knott, P. A. & Dunningham, J. A. Multiparameter estimation in networked quantum sensors. *Phys. Rev. Lett.* **120**, 080501 (2018).
11. Raussendorf, R. & Briegel, H. J. A one-way quantum computer. *Phys. Rev. Lett.* **86**, 5188–5191 (2001).
12. Walther, P. et al. Experimental one-way quantum computing. *Nature* **434**, 169–176 (2005).
13. Broadbent, A., Fitzsimons, J. & Kashefi, E. Universal blind quantum computation. In *Proceedings of the 2009 50th Annual IEEE Symposium on Foundations of Computer Science*, FOCS '09, 517–526 (IEEE Computer Society, 2009).
14. Barz, S. et al. Demonstration of blind quantum computing. *Science* **335**, 303–308 (2012).
15. Chen, K. & Lo, H.-K. Multi-partite quantum cryptographic protocols with noisy GHZ states. *Quantum Inf. Comput.* **7**, 689–715 (2007).
16. Lo, H.-K., Curty, M. & Tamaki, K. Secure quantum key distribution. *Nat. Photonics* **8**, 595 (2014).
17. Epping, M., Kampermann, H., Macchiavello, C. & Bruß, D. Multi-partite entanglement can speed up quantum key distribution in networks. *N. J. Phys.* **19**, 093012 (2017).
18. Northup, T. E. & Blatt, R. Quantum information transfer using photons. *Nat. Photonics* **8**, 356 (2014).
19. Monroe, C. et al. Large-scale modular quantum-computer architecture with atomic memory and photonic interconnects. *Phys. Rev. A* **89**, 022317 (2014).
20. Reiserer, A. & Rempe, G. Cavity-based quantum networks with single atoms and optical photons. *Rev. Mod. Phys.* **87**, 1379–1418 (2015).
21. Sipahigil, A. et al. An integrated diamond nanophotonics platform for quantum-optical networks. *Science* **354**, 847–850 (2016).
22. Kalb, N. et al. Entanglement distillation between solid-state quantum network nodes. *Science* **356**, 928–932 (2017).
23. Pirker, A., Wallnöfer, J. & Dür, W. Modular architectures for quantum networks. *N. J. Phys.* **20**, 053054 (2018).
24. Humphreys, P. C. et al. Deterministic delivery of remote entanglement on a quantum network. *Nature* **558**, 268–273 (2018).
25. Chou, K. S. et al. Deterministic teleportation of a quantum gate between two logical qubits. *Nature* **561**, 368–373 (2018).
26. Jing, B. et al. Entanglement of three quantum memories via interference of three single photons. *Nat. Photonics* **13**, 210–213 (2019).
27. Yu, Y. et al. Entanglement of two quantum memories via fibres over dozens of kilometres. *Nature* **578**, 240–245 (2020).
28. Stephenson, L. J. et al. High-rate, high-fidelity entanglement of qubits across an elementary quantum network. *Phys. Rev. Lett.* **124**, 110501 (2020).
29. Awschalom, D. et al. Development of quantum interconnects (quics) for next-generation information technologies. *PRX Quantum* **2**, 017002 (2021).

30. Pompili, M. et al. Realization of a multinode quantum network of remote solid-state qubits. *Science* **372**, 259–264 (2021).
31. Lago-Rivera, D., Grandi, S., Rakonjac, J. V., Seri, A. & de Riedmatten, H. Telecom-heralded entanglement between multimode solid-state quantum memories. *Nature* **594**, 37–40 (2021).
32. Hermans, S. L. N. et al. Qubit teleportation between non-neighbouring nodes in a quantum network. *Nature* **605**, 663–668 (2022).
33. van Leent, T. et al. Entangling single atoms over 33 km telecom fibre. *Nature* **607**, 69–73 (2022).
34. Pompili, M. et al. Experimental demonstration of entanglement delivery using a quantum network stack. *npj Quantum Inf.* **8**, 121 (2022).
35. Krutyanskiy, V. et al. Entanglement of trapped-ion qubits separated by 230 meters. *Phys. Rev. Lett.* **130**, 050803 (2023).
36. Knaut, C. M. et al. Entanglement of nanophotonic quantum memory nodes in a telecom network. *Nature* **629**, 573–578 (2024).
37. Ruskuc, A. et al. Scalable multipartite entanglement of remote rare-earth ion qubits. Preprint at https://arxiv.org/abs/2402.16224 (2024).
38. Li, C.-M. et al. Genuine high-order Einstein-Podolsky-Rosen steering. *Phys. Rev. Lett.* **115**, 010402 (2015).
39. Huang, C.-Y., Lambert, N., Li, C.-M., Lu, Y.-T. & Nori, F. Securing quantum networking tasks with multipartite einstein-podolsky-rosen steering. *Phys. Rev. A* **99**, 012302 (2019).
40. Lu, H. et al. Counting classical nodes in quantum networks. *Phys. Rev. Lett.* **124**, 180503 (2020).
41. Tóth, G. & Gühne, O. Detecting genuine multipartite entanglement with two local measurements. *Phys. Rev. Lett.* **94**, 060501 (2005).
42. Horodecki, R., Horodecki, P., Horodecki, M. & Horodecki, K. Quantum entanglement. *Rev. Mod. Phys.* **81**, 865–942 (2009).
43. Gühne, O. & Tóth, G. Entanglement detection. *Phys. Rep.* **474**, 1 – 75 (2009).
44. McCutcheon, W. et al. Experimental verification of multipartite entanglement in quantum networks. *Nat. Commun.* **7**, 13251 (2016).
45. Han, Y.-G., Li, Z., Wang, Y. & Zhu, H. Optimal verification of the bell state and greenberger–horne–zeilinger states in untrusted quantum networks. *npj Quantum Inf.* **7**, 164 (2021).
46. Kaniewski, J. Analytic and nearly optimal self-testing bounds for the clauser-horne-shimony-holt and mermin inequalities. *Phys. Rev. Lett.* **117**, 070402 (2016).
47. Baccari, F., Augusiak, R., Šupić, I., Tura, J. & Acín, A. Scalable bell inequalities for qubit graph states and robust self-testing. *Phys. Rev. Lett.* **124**, 020402 (2020).
48. Wu, D. et al. Closing the locality and detection loopholes in multiparticle entanglement self-testing. *Phys. Rev. Lett.* **128**, 250401 (2022).
49. He, Q. Y. & Reid, M. D. Genuine multipartite einstein-podolsky-rosen steering. *Phys. Rev. Lett.* **111**, 250403 (2013).
50. Armstrong, S. et al. Multipartite einstein–podolsky–rosen steering and genuine tripartite entanglement with optical networks. *Nat. Phys.* **11**, 167–172 (2015).
51. Cavalcanti, D. et al. Detection of entanglement in asymmetric quantum networks and multipartite quantum steering. *Nat. Commun.* **6**, 7941 (2015).
52. Tavakoli, A., Pozas-Kerstjens, A., Luo, M.-X. & Renou, M.-O. Bell nonlocality in networks. *Rep. Prog. Phys.* **85**, 056001 (2022).
53. Sun, Q.-C. et al. Experimental demonstration of non-bilocality with truly independent sources and strict locality constraints. *Nat. Photonics* **13**, 687–691 (2019).
54. Poderini, D. et al. Experimental violation of n-locality in a star quantum network. *Nat. Commun.* **11**, 2467 (2020).
55. Suprano, A. et al. Experimental genuine tripartite nonlocality in a quantum triangle network. *PRX Quantum* **3**, 030342 (2022).
56. Gu, X.-M. et al. Experimental full network nonlocality with independent sources and strict locality constraints. *Phys. Rev. Lett.* **130**, 190201 (2023).
57. Bell, B. A. et al. Experimental characterization of universal one-way quantum computing. *N. J. Phys.* **15**, 053030 (2013).
58. Miguel-Ramiro, J., Pirker, A. & Dür, W. Genuine quantum networks with superposed tasks and addressing. *npj Quantum Inf.* **7**, 135 (2021).
59. Hein, M., Eisert, J. & Briegel, H. J. Multiparty entanglement in graph states. *Phys. Rev. A* **69**, 062311 (2004).
60. Bourennane, M. et al. Experimental detection of multipartite entanglement using witness operators. *Phys. Rev. Lett.* **92**, 087902 (2004).
61. Gühne, O., Lu, C.-Y., Gao, W.-B. & Pan, J.-W. Toolbox for entanglement detection and fidelity estimation. *Phys. Rev. A* **76**, 030305 (2007).
62. Zhang, S. et al. Quantum-memory-enhanced preparation of nonlocal graph states. *Phys. Rev. Lett.* **128**, 080501 (2022).
63. Appel, M. H. et al. Entangling a hole spin with a time-bin photon: A waveguide approach for quantum dot sources of multiphoton entanglement. *Phys. Rev. Lett.* **128**, 233602 (2022).
64. Brunner, N., Cavalcanti, D., Pironio, S., Scarani, V. & Wehner, S. Bell nonlocality. *Rev. Mod. Phys.* **86**, 419–478 (2014).
65. Mermin, N. D. Hidden variables and the two theorems of john bell. *Rev. Mod. Phys.* **65**, 803–815 (1993).
66. Gühne, O., Tóth, G., Hyllus, P. & Briegel, H. J. Bell inequalities for graph states. *Phys. Rev. Lett.* **95**, 120405 (2005).
67. Pan, J.-W., Daniell, M., Gasparoni, S., Weihs, G. & Zeilinger, A. Experimental demonstration of four-photon entanglement and high-fidelity teleportation. *Phys. Rev. Lett.* **86**, 4435–4438 (2001).
68. Pan, J.-W. et al. Multiphoton entanglement and interferometry. *Rev. Mod. Phys.* **84**, 777–838 (2012).
69. Hong, C. K., Ou, Z. Y. & Mandel, L. Measurement of subpicosecond time intervals between two photons by interference. *Phys. Rev. Lett.* **59**, 2044–2046 (1987).

Acknowledgements

We thank S.-L. Chen, Y.-N. Chen, Y.-A. Chen, and J.-W. Pan for helpful comments and discussions. C.-Y. Huang was partially supported by the MOE Taiwan-Caltech Fellowship. This work was partially supported by the National Science and Technology Council, Taiwan, under Grant Numbers MOST 107-2628-M-006-001-MY4, MOST 111-2112-M-006-033, MOST 111-2119-M-007-007, MOST 111-2123-M-006-001, and NSTC 112-2112-M-006-029.

Author contributions

W.-T.K. and C.-Y.H. contributed equally to this work. W.-T.K., T.-J.T., S.-H.C., S.-Y.S., and C.-M.L. designed the experiment. C.-Y.H. and C.-M.L. established the final theoretical framework. C.-Y.H., W.-T.K., T.-L.L., and C.-M.L. performed the theoretical calculations. W.-T.K., T.-J.T., S.-H.C., S.-Y.S., and Y.-C.L. performed the experiment. W.-T.K., T.-J.T., S.-H.C., S.-Y.S., Y.-C.L., C.-S.C., H.L., and C.-M.L. analyzed the data. C.-Y.H. and C.-M.L. wrote the paper, and all authors contributed to the editing of the manuscript. C.-M.L. devised the basic model and supervised the project.

Competing interests

The authors declare no competing interests.

Additional information

Supplementary information The online version contains supplementary material available at https://doi.org/10.1038/s41534-024-00867-0.

Correspondence and requests for materials should be addressed to Che-Ming Li.